IEEE Access
Multidisciplinary | Rapid Review | Open Access Journal

Received October 12, 2021, accepted October 27, 2021, date of publication November 4, 2021, date of current version November 15, 2021.

Digital Object Identifier 10.1109/ACCESS.2021.3125501

High-Precision Positioning Method of Coal Shearer in the Underground Environment Based on Rail Kinematics Model

XIAOWEI XU[1], JIZHOU LAI[1], PIN LV[1], JUNQING LU[2], SHIYU BAI[1], AND HUAFENG HU[2]
[1]College of Automation, Nanjing University of Aeronautics and Astronautics, Nanjing 211000, China
[2]Hubei Academy of Spaceflight Technology, Wuhan 430040, China

Corresponding author: Jizhou Lai (laijz@nuaa.edu.cn)

This work was supported in part by the National Natural Science Foundation of China under Grant 61973160 and Grant 61703207, in part by the Aeronautical Science Foundation of China under Grant 2018ZC52037, in part by the Civil Aircraft Project of Ministry of Industry and Information under Grant 2018-S-36, and in part by the Basic Research Program under Grant 51405-02B02.

ABSTRACT The high-precision positioning of the shearer is the key technology to realize the automation of longwall mining. Since mine is a Global Position System (GPS)-denied environment, highly autonomous Inertial Navigation System (INS)/odometer integrated navigation has been widely used. At present, the shearer positioning method based on INS/odometer has been challenging to meet the requirements of long-time and high-precision mining. Aiming at the high-precision navigation in the complex mining environment, this paper constructs a comprehensive rail kinematics model of the shearer that does not rely on external sensors. By analyzing the kinematic characteristics of the shearer and the scraper conveyor during the longwall mining process, a method of information fusion and navigation system fault diagnosis based on the assistance of the shearer rail kinematics model was proposed. According to the working principle of the shearer rails and hydraulic supports, the characteristics of the trajectory deviation caused by the sensor fault of the hydraulic support are analyzed. Combined with the engineering requirements of shearer mining, the model fault identification was carried out by the fading probability ratio detection algorithm. The simulation results show that the proposed algorithm effectively improves the positioning of shearer accuracy in multiple cutting cycles. At the same time, it avoids the influence of the rail deviation caused by the rail kinematics model fault on the positioning of the shearer.

INDEX TERMS Underground environment, shearer, rail kinematics model, information fusion, autonomous navigation, fault detection.

I. INTRODUCTION

Coal is the primary fossil energy and plays a vital role in the world energy structure. Because the mine is a closed environment, explosive gas and dust can easily lead to coal mine safety accidents [1]. Since the U.S. Bureau of Mines proposed computer-aided coal mining technology in the 1980s, the high-precision autonomous positioning of underground shearers has become a significant technical challenge in the process of automation [2].

Inertial navigation system (INS) is widely used to position underground equipment due to its highly autonomous and reliable navigation performance. As early as the 1980s, Sammacro [3] developed a navigation system based on gyroscopes, magnetic heading sensors, and inclinometers to measure the attitude of underground mine equipment for autonomous mining operations. However, INS inevitably has error divergence when it calculates position and attitude through numerical product, which is the inherent limitation. Therefore, the inertial error is usually corrected through external information. Reid *et al.* [4] utilized the motion characteristics of the sharer, the accumulated errors of the INS are corrected by zero velocity update (ZUPT). Although the ZUPT is simple and easy to implement, the shearer needs to be stopped periodically. Whenever the shearer starts moving, errors will continue to accumulate.

The long-term positioning accuracy of the odometer is better than INS. Meanwhile, the odometer has excellent autonomy and stability. Therefore, the integrated navigation of INS/odometer is the primary method for coal shearer positioning. Wang and Wang [5] utilized the position and speed information to fuse through information filtering, which

The associate editor coordinating the review of this manuscript and approving it for publication was Resul Das.

significantly improved the positioning accuracy of the shearer compared with the pure inertial positioning. Ralston *et al.* [6] earlier put forward the conception of using a wireless sensor network to locate underground mine mobile equipment. Fan *et al.* [7] positioned the shearer by using the time of arrival (TOA) positioning method through the UWB base station installed on the hydraulic support and labels installed on the shearer, which effectively reduces the positioning error of INS. To solve the mixed line-of-sight and non-line-of-sight errors caused by underground environmental barriers, Cao *et al.* [8] proposed an interactive multi-model algorithm based on the Gaussian mixture model to reduce the frequent switching between line-of-sight and non-line-of-sight scenes. However, it is difficult to install and calibrate the base station used for shearer positioning. The label may not always receive the base station signal due to the occlusion in the positioning process. In addition, researchers have also conducted extensive studies on visual perception methods [9], infrared radiation methods [10], Doppler velocimetry method [11], and other methods [12]. Since active sensing sensors are usually affected by the complex environment of the shearer's working face, their availability and reliability are difficult to guarantee.

To meet the positioning requirements of GPS-denied environment, the Commonwealth Scientific and Industrial Research Organization (CSIRO) in Australia has proposed a closed path based reverse correction method [13]. On this basis, Shibo *et al.* [14] established the rail kinematics model to assist positioning according to the motion characteristics of the shearer on the scraper conveyor and improved the navigation accuracy of the shearer through Kalman filtering theory without relying on external sensors. Due to the lack of further analysis on the mechanical structure of the scraper conveyor in the mining process, the engineering value of the algorithm is affected.

The rest of this paper is organized as follows: Firstly, a Refinement model of shearer rail is constructed in section II. The integration navigation strategy is presented in section III, which analyses the construction of system model, measurement model, and federated filtering architecture in the work. A fault detection method of rail kinematics model based on the fading sequential probability ratio detection algorithm is proposed in section IV. In section V, the algorithm is verified by experiment and simulation. The conclusion is summarized in section VI.

II. REFINEMENT MODEL OF SHEARER RAIL

Comprehensive mechanized coal mining is a process of coal mining using mechanized and automated equipment. Fully mechanized mining equipment mainly includes shearer, scraper conveyor, and hydraulic support [15]. In the cutting process, the shearer breaks the coal along the horizontal direction of the working face first. After the coal seam falls off, the scraper conveyor transports the coal to the crusher. In the cutting process of the shearer, the hydraulic support will ensure that the top coal will not collapse and control the longitudinal mining depth of the working face in the next cycle. Usually, according to the actual situation of the coal seam, the hydraulic support will push the roof support system and scraper conveyor after 0.8-1m thick coal body is cut down by the shearer. The scraper conveyor is used to transport coal and materials and the rail of the shearer, so the movement of the shearer is consistent with the track of the scraper conveyor. The circular cutting track and scraper conveyor structure are shown in Fig. 2. The longitudinal distance between each cutting surface (point A to B) can be measured by the displacement sensor of the shearer's hydraulic support. The horizontal plane of the rail kinematics model is controlled by many hydraulic supports, therefore a certain error exists between each chute, resulting in the included angle between chutes. Since each chute is a rigid body, the movement trajectory of the shearer should be a broken line that conforms to the movement characteristics of the scraper conveyor [16].

III. INS/ODOMETER HIGH-PRECISION POSITIONING ALGORITHM ASSISTED BY RAIL KINEMATICS MODEL

According to the cutting process of the shearer, the current cutting trajectory can be predicted according to the rail kinematics model based on the trajectory of the last cutting, and the position measurement of the current shearer can be obtained. The constraint information of the rail kinematics model is integrated with the traditional INS/odometer. The system model, measurement model, and fusion framework are constructed as Fig 1 and Fig 2:

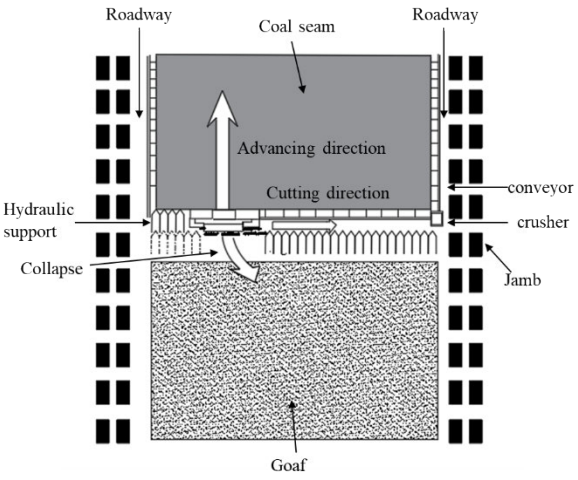

FIGURE 1. Schematic diagram of the longwall fully mechanized mining process.

A. SYSTEM MODEL CONSTRUCTION

This paper is based on the east-north-up (ENU) coordinate system. The coordinates and attitude angles are shown in Fig. 3; the specific structure is shown in Fig. 4.

The angle between the projection Y_b' of the carrier Y_b on the navigation coordinate system $X_N - O - Y_N$ plane and the

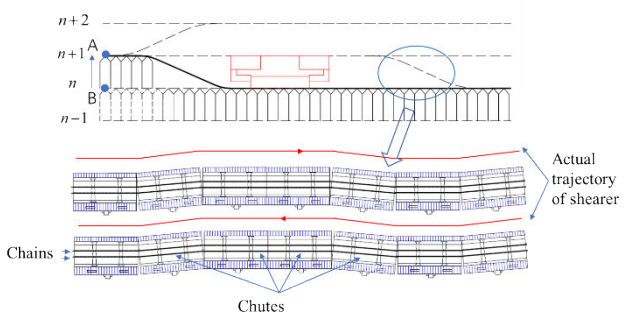

FIGURE 2. Shearer cutting motion track.

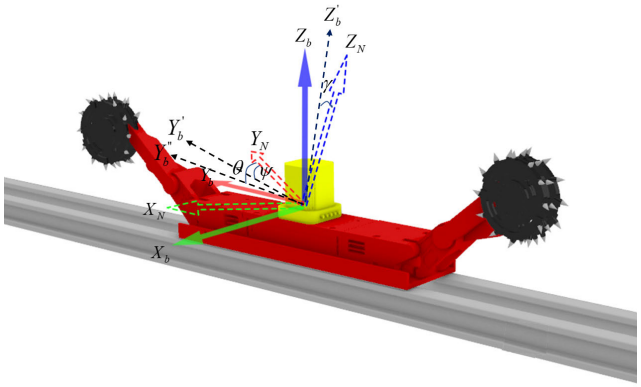

FIGURE 3. INS/odometer/rail kinematics model positioning scheme: (N) is the ENU navigation coordinate and (b) is the body coordinate.

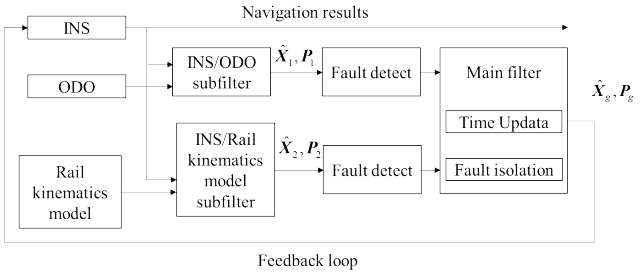

FIGURE 4. The optimal estimation and detection algorithm structure based on the rail kinematics model.

geographic north Y_N is the heading angle ψ. The value starts from Y_N on $X_N - O - Y_N$ plane and the domain of definition is 0° to 360°. The angle between the geographic north Y_N and the projection Y_b'' of carrier Y_b on the navigation coordinate system $Z_N - O - Y_N$ plane is the pitch angle θ, which produced by the rotation of the carrier around the horizontal axis X_b. Reference to coordinate system $Z_N - O - Y_N$ plane, the pitch angle is positive for upwards and negative for downwards. The domain of definition is −90° to 90°. The angle between the projection Z_b' of the carrier Z_b on the navigation coordinate system $Z_N - O - X_N$ plane and the navigation coordinate system Z_N axis is defined as the roll angle γ. Reference to the coordinate system $Z_N - O - X_N$ plane, right tilt is positive, left tilt is negative, and the domain of definition is −180° to 180°.

The error equations of strapdown INS are selected as the state equations of the integrated navigation system. The odometer scale factor error and installation error also need to be considered. The state values are set as follows:

$$\boldsymbol{X}_k = \begin{bmatrix} \boldsymbol{\phi} & \delta\boldsymbol{v} & \delta\boldsymbol{p} & \boldsymbol{\varepsilon}_b & \boldsymbol{\varepsilon}_r & \boldsymbol{\nabla} & s \end{bmatrix}$$

where, $\boldsymbol{\phi} = \begin{bmatrix} \varphi_E & \varphi_N & \varphi_U \end{bmatrix}$ is the platform error angle, $\delta\boldsymbol{v} = \begin{bmatrix} \delta v_E & \delta v_N & \delta v_U \end{bmatrix}$ is the east, north and vertical velocity error of the carrier. $\delta\boldsymbol{p} = \begin{bmatrix} \delta\lambda & \delta L & \delta h \end{bmatrix}$ is the longitude, latitude and height errors of the carrier, respectively. $\boldsymbol{\varepsilon}_b = \begin{bmatrix} b_{bx} & b_{by} & b_{bz} \end{bmatrix}$ is the 3-axis gyroscope random constant [17]. $\boldsymbol{\varepsilon}_r = \begin{bmatrix} \varepsilon_{rx} & \varepsilon_{ry} & \varepsilon_{rz} \end{bmatrix}$ is the first-order Markov process random noise of the 3-axis gyroscope. Because the zero bias of the accelerometer is trivial and relatively stable, it can be calibrated through the turntable. To reduce the amount of calculation, the random constant of the accelerometer is not modeled. $\boldsymbol{\nabla} = \begin{bmatrix} \nabla_x & \nabla_y & \nabla_z \end{bmatrix}$ is the first-order Markov process random noise of the 3-axis accelerometer. s is the scale factor error of the odometer. According to the error equation of navigation system [16], the state equation is obtained:

$$\boldsymbol{X}_k = \boldsymbol{\Phi}_{k|k-1}\boldsymbol{X}_{k-1} + \boldsymbol{G}_{k-1}\boldsymbol{W}_{k-1} \tag{1}$$

where, the subscripts k and $k-1$ stand for the sampling time index. $\boldsymbol{\Phi}_{k|k-1}$ is the one-step transfer matrix of the system, $\boldsymbol{G}_{k-1}$ is the system noise matrix, and $\boldsymbol{W}_{k-1}$ is the system noise.

B. MEASUREMENT MODEL CONST RUCTION

According to the movement characteristics of the shearer, there are multiple moments of static state in the cutting process of the shearer, and the cumulative error of the speed can be corrected periodically through zero speed correction. The measurement equation is as follows:

$$\begin{aligned} \boldsymbol{Z}_{ZUPT,k} &= \boldsymbol{H}_{ZUPT,k}\boldsymbol{X}_k + \boldsymbol{V}_{ZUPT,k} \\ &= \begin{bmatrix} v_{IE} - 0 \\ v_{IN} - 0 \\ v_{IU} - 0 \end{bmatrix} = \begin{bmatrix} \delta v_E \\ \delta v_N \\ \delta v_U \end{bmatrix} + \begin{bmatrix} w_{ZUPT1} \\ w_{ZUPT2} \\ w_{ZUPT3} \end{bmatrix} \\ &= \begin{bmatrix} 0_{3\times3} & diag\begin{bmatrix} 1 & 1 & 1 \end{bmatrix} & 0_{3\times13} \end{bmatrix}\boldsymbol{X}_k + \begin{bmatrix} w_{ZUPT1} \\ w_{ZUPT2} \\ w_{ZUPT3} \end{bmatrix} \end{aligned} \tag{2}$$

where $Z_{ZUPT,k}$ is the difference between the measurement information of zero velocity correction and the velocity information of the INS, $H_{ZUPT,k}$ is the measurement coefficient matrix, and $V_{ZUPT,k}$ is the measurement noise.

The odometer is a kind of sensor that can provide the distance relative to the initial position and has better long-term accuracy than INS. According to the working principle of

the shearer walking device, the equipped odometer can only provide the forward pulse of the body coordinate. The current position of the shearer can be obtained through the scale factor of the odometer pulse and the attitude information provided by the INS. The measurement model is as follows:

$$\begin{aligned}\boldsymbol{P}_{O,k} &= \boldsymbol{P}_{O,k-1} + \boldsymbol{C}_{b\,k-1}^{n}\Delta\boldsymbol{d}_{C,k-1} \\ &= \boldsymbol{P}_{O,k-1} + \boldsymbol{C}_{b\,k-1}^{n}((p-\Delta p)M_k - (p-\Delta p)M_{k-1})\end{aligned} \tag{3}$$

where M_k and M_{k-1} are the number of pulses. $\boldsymbol{P}_{O,k}$ and $\boldsymbol{P}_{O,k-1}$ are the position of the shearer under the navigation system. $\boldsymbol{C}_b^n$ is the attitude transfer matrix, p and Δp are the true value of the scale factor and the error of the scale factor of the odometer. The measurement equation is:

$$\begin{aligned}\boldsymbol{Z}_{O,k} &= \boldsymbol{H}_{O,k}\boldsymbol{X}_k + \boldsymbol{V}_{O,k} \\ &= \begin{bmatrix} L_{IE}-L_{OE} \\ \lambda_{IN}-\lambda_{ON} \\ h_{IU}-h_{OU}\end{bmatrix} = \begin{bmatrix}\delta L_E \\ \delta\lambda_N \\ \delta h_U\end{bmatrix} + \begin{bmatrix} w_{O1} \\ w_{O2} \\ w_{O3}\end{bmatrix} \\ &= \begin{bmatrix} 0_{1\times6} & R_m & 0 & 0 & 0_{1\times9} & -\Delta M\cos\psi\cos\theta \\ 0_{1\times6} & 0 & R_n\cos L & 0 & 0_{1\times9} & -\Delta M\sin\psi\cos\theta \\ 0_{1\times6} & 0 & 0 & 1 & 0_{1\times9} & -\Delta M\sin\theta\end{bmatrix}\boldsymbol{X}_k \\ &\quad + \begin{bmatrix} w_{O1} \\ w_{O2} \\ w_{O3}\end{bmatrix}\end{aligned} \tag{4}$$

where $Z_{O,k}$ is the difference between the position measurement of odometer and the position of INS, $H_{O,k}$ is the measurement coefficient matrix of odometer, $V_{O,k}$ is the measurement noise. L, λ and h represent longitude, latitude and altitude, respectively. θ and ψ represent the pitch angle and the heading angle, respectively. R_M and R_N are the radius of curvature of the earth's meridian circle and the unitary circle, and ΔM is the difference of pulse number at continuous time.

According to the rail kinematics model, the trajectory position information of the current cutting shearer can be predicted. Different working conditions will lead to different speeds of the shearer in each cutting cycle. When the shearer moves over a fixed distance, the expected point of the rail kinematics model matches the estimated point of the current position. The measurement model is constructed as follows:

$$P_{CE,k} = P_{CE,k-1} + d_{C,k-1}\sin(\psi) + w_{CE,k} \tag{5}$$

$$P_{CN,k} = P_{CN,k-1} + d_{C,k-1}\cos(\psi) + w_{CN,k} \tag{6}$$

where, $P_{CE,k}$ and $P_{CN,k}$ are respectively the east and north position of shearer given by the rail kinematics model; $d_{C,k-1}$ is the advancing distance of shearer hydraulic support relative to the vertical direction of the working face; $w_{CE,k}$ and $w_{CN,k}$ is the position noise of chute.

$$w_{CE,k} = r_{i,k}\sin(o_i)\sin(\psi) + b_i \tag{7}$$

$$w_{CN,k} = r_{i,k}\sin(o_i)\cos(\psi) + b_i \tag{8}$$

where, $r_{i,k}$ is the distance that the shearer moves in the chute, o is the angle between the chute and the horizontal cutting surface of the shearer. b_i is the noise measured by the displacement sensor [18]. The measurement equation is as follows:

$$\begin{aligned}\boldsymbol{Z}_{C,k} &= \boldsymbol{H}_{C,k}\boldsymbol{X}_k + \boldsymbol{V}_{C,k} \\ &= \begin{bmatrix}(L_{IE}-L_{CE})R_m \\ (\lambda_{IE}-\lambda_{CE})R_n\cos L\end{bmatrix} = \begin{bmatrix}R_m\delta L \\ R_n\cos L\delta\lambda\end{bmatrix} + \begin{bmatrix} w_{CE} \\ w_{CN}\end{bmatrix} \\ &= \begin{bmatrix} 0_{1\times6} & R_m & 0 & 0_{1\times11} \\ 0_{1\times6} & 0 & R_n\cos L & 0_{1\times11}\end{bmatrix}\boldsymbol{X}_k + \begin{bmatrix} w_{CE} \\ w_{CN}\end{bmatrix}\end{aligned} \tag{9}$$

where, $Z_{C,k}$ is the difference between the measurement of the rail kinematics model and the output position of INS. $H_{C,k}$ and $V_{C,k}$ are the measurement coefficient matrix and measurement noise of the rail kinematics model, respectively.

Federated filter is a two-stage data fusion structure consisting of several sub-filters working in parallel to complete Kalman filter calculation. In this paper, two sub-filters based on INS/odometer and INS/rail kinematics model are designed. The INS/odometer sub-filter and the INS/rail kinematics model sub-filter are corrected by position of odometer output and the rail kinematics model output respectively, and the ZUPT is carried out when the cutting stops. The information fusion of inertial state recursion and measurement is carried out by EKF respectively [19]. Then, the local estimations and the corresponding covariances are fused by a global filter to obtain the global optimal estimation. The information fusion equation is as follows:

$$\boldsymbol{P}_g = \left(\sum_{j=1}^{N}\boldsymbol{P}_j^{-1}\right)^{-1} \tag{10}$$

$$\hat{\boldsymbol{X}}_g = \mathbf{P}_g\left(\sum_{j=1}^{N}\boldsymbol{P}_j^{-1}\hat{\boldsymbol{X}}_j\right) \tag{11}$$

where $\boldsymbol{P}_g$ is the covariance matrix of the estimated state, $\boldsymbol{P}_j$ corresponds to the estimated error covariance matrix of each sub-filter, $\hat{\boldsymbol{X}}_g$ is the global optimal estimation result, $\hat{\boldsymbol{X}}_j$ is the state estimation of the sub-filter, N represents the number of sub-filters, j stands for the j-th sub-filter [20].

IV. FAULT DIAGNOSIS OF RAIL KINEMATICS MODEL BASED ON FEDERATED FILTER

The scraper conveyor of the shearer is usually controlled by nearly 200 hydraulic supports. If the sensors of hydraulic supports fail and the faults are not timely isolated, the accuracy of the rail kinematics model will decrease. According to the mining regulations of the shearer, the scraper conveyor needs to maintain the horizontal bending angle of each chute and the horizontal cutting trajectory deviation should be less than the index requirements of the scraper conveyor. In this paper, a fault detection algorithm of fading probability ratio based on the federated filter is proposed.

A. FADING PROBABILITY RATIO FAULT DETECTION MODEL BASED ON FEDERATED FILTER

The rail kinematics model caused by the fault of the hydraulic support measurement sensor is shown in Fig. 5.

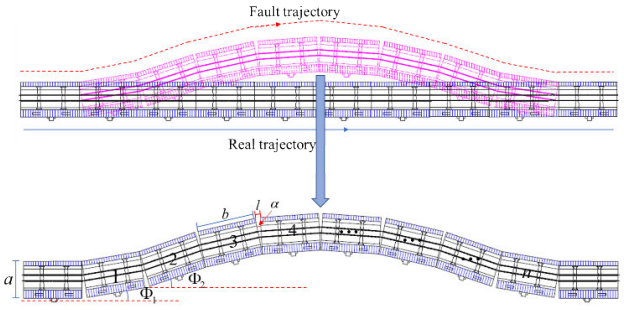

FIGURE 5. Schematic diagram of rail kinematics model.

The discrete measurement model of federated filter sub-filter under fault is as follows:

$$\boldsymbol{Z}_{C,k} = \boldsymbol{H}(k)\boldsymbol{X}_k + \boldsymbol{V}_{C,k} + \boldsymbol{f}_{C,k} \tag{12}$$

where, $\boldsymbol{H}_{C,k}$ is the measurement matrix of the subsystem, $\boldsymbol{V}_{C,k}$ is the measurement noise, and $\boldsymbol{f}_{C,k}$ is the fault information. According to the rail kinematics model, the fault information model is as follows:

$$\begin{aligned}\boldsymbol{f}_{C,k} = \boldsymbol{C}_b^n((l+b)\sin\Phi_1 + (l+b)\sin\Phi_2 \\ + \cdots + (l+b)\sin\Phi_n)\end{aligned} \tag{13}$$

where, Φ is the included angle between each chute of the bending section and the longitudinal line (coal wall line of the mining face) of the scraper conveyor, b is the length of each chute, l is the chord length corresponding to the horizontal included angle α between the chute of the bending section. Because of the small value of α, the chord length and arc length can be regarded as equal, l can be expressed as:

$$l = \frac{\pi a \alpha}{180} \tag{14}$$

The innovation value of the sub-filter at time k can be obtained by the following formula:

$$\boldsymbol{V}_k = \boldsymbol{Z}_k - \boldsymbol{H}_k\hat{\boldsymbol{X}}_{k/k-1} = \boldsymbol{v}_k + \boldsymbol{\zeta}_k \tag{15}$$

where $\boldsymbol{\zeta}_k$ is the system disturbance. When the system is not disturbed, the continuous-time innovation sequence sample is $\{v_1\ v_2\ \cdots\ v_k\}$, the sample satisfies $\boldsymbol{v} \sim \mathrm{N}(\bar{\boldsymbol{v}}_k, \boldsymbol{\sigma}_k)$, $\bar{\boldsymbol{v}}$ is the sample mean, $\boldsymbol{\sigma}_k^2$ is the sample variance. The variance of the sub-filter can be obtained by the following formula:

$$\boldsymbol{\sigma}_k^2 = \boldsymbol{H}_k\boldsymbol{P}_{k/k-1}\boldsymbol{H}_k^T + \boldsymbol{R}_k \tag{16}$$

where $\boldsymbol{P}_{k/k-1}$ is the one-step prediction mean square error, $\boldsymbol{R}_k$ is measurement noise.

In the fault analysis of an integrated navigation system, the binary hypothesis is usually made for the mean value of the innovation sequence $\bar{v}$ of the sub-filter:

$$\begin{cases} H_0 = \bar{\boldsymbol{v}} = 0 & 0 \\ H_1 = \bar{\boldsymbol{v}} \neq 0 & 1 \end{cases} \tag{17}$$

where H_0 and H_1 represent system fault and fault free, respectively.

According to the above formula, the prior probability under the binary fault hypothesis is as follows:

$$p(\boldsymbol{v}_k \mid H_0) = \frac{1}{\sqrt{2\pi}\boldsymbol{\sigma}_k}\exp\left[-\frac{1}{2}(\frac{\boldsymbol{v}_k}{\boldsymbol{\sigma}_k})^2\right] \tag{18}$$

$$p(\boldsymbol{v}_k \mid H_1) = \frac{1}{\sqrt{2\pi}\boldsymbol{\sigma}_k}\exp\left[-\frac{1}{2}(\frac{\boldsymbol{v}_k - \boldsymbol{\xi}_k}{\boldsymbol{\sigma}_k})^2\right] \tag{19}$$

According to the maximal posterior probability criterion, the likelihood ratio of the innovation sequence samples in continuous time is as follows:

$$\begin{aligned}\lambda_k &= \ln(\prod_{k=1}^{k}\frac{p(\boldsymbol{v}_k \mid H_1)}{p(\boldsymbol{v}_k \mid H_0)}) \\ &= \ln\left[\prod_{k=1}^{k-1}\frac{p(\boldsymbol{v}_k \mid H_1)}{p(\boldsymbol{v}_k \mid H_0)}\right] + \ln\left[\frac{p(\boldsymbol{v}_k \mid H_1)}{p(\boldsymbol{v}_k \mid H_0)}\right] \\ &= \sum_{k-1=1}^{k-1}\frac{(\boldsymbol{v}_{k-1} - \bar{\boldsymbol{v}}_{k-1})^{\mathrm{T}}(\boldsymbol{v}_{k-1} - \bar{\boldsymbol{v}}_{k-1}) - \boldsymbol{v}_{k-1}^{\mathrm{T}}\boldsymbol{v}_{k-1}}{2\boldsymbol{\sigma}_{k-1}^2} \\ &\quad + \frac{(\boldsymbol{v}_k - \bar{\boldsymbol{v}}_k)^{\mathrm{T}}(\boldsymbol{v}_k - \bar{\boldsymbol{v}}_k) - \boldsymbol{v}_k^{\mathrm{T}}\boldsymbol{v}_k}{2\boldsymbol{\sigma}_k^2} \\ &= \lambda_{k-1} + \Delta\lambda_k\end{aligned} \tag{20}$$

It can be seen from the above formula that as k increases, the proportion of the mean value of the innovation sample $\bar{v}_k$ becomes smaller and smaller. Since the sensitivity of the detection algorithm is constantly decreasing, the weight of the historical sample mean is reduced by introducing a fading factor, thereby improving the sensitivity of the detection algorithm. The mean value of the innovation sample after introducing the fading factor is as follows [21], [22]:

$$d_k = \frac{1-b}{1-b^k} \tag{21}$$

$$\bar{\boldsymbol{v}} = (1-d_k)\sum_{k-1=1}^{k-1}\boldsymbol{v}_{k-1} + d_k\boldsymbol{v}_k \tag{22}$$

where, b is the fading factor.

The statistic is as follows:

$$\lambda_k = \sum_{k-1=1}^{k-1} b\lambda_{k-1} + \Delta\lambda_k \tag{23}$$

Fault detection criteria are as follows:

$$J = \begin{cases} \lambda_k > T1 \\ \lambda_k \leqslant T0 \end{cases} \tag{24}$$

where T is the threshold. $j = 1$ means that the rail kinematics model is faulty. $j = 0$ means that the rail kinematics model is faulty-free.

V. EXPERIMENTS

A. SIMULATION VERIFICATION

To verify the effectiveness of the algorithm proposed in this paper, a simulation experiment is carried out. According to the actual working conditions of the shearer, a 360m working

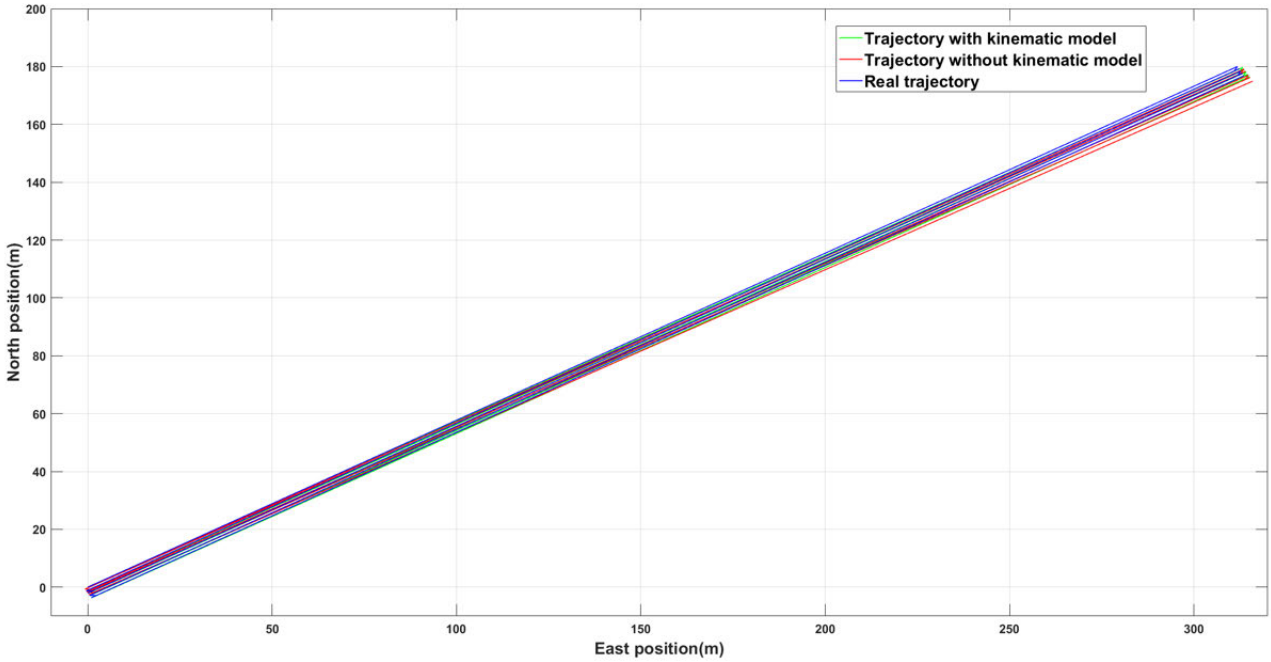

FIGURE 6. Comparison of shearer horizontal cutting trajectory.

TABLE 1. Simulation setting of main sensors.

Sensors	Performance parameters
INS	Zero-bias stability of gyro 0.001deg/h Angle random walk of gyro 0.0001deg/sqrt(h) Zero-bias stability of Accelerometers 30 μg
Odometer	Scale factor error 3‰
Rail kinematics model	Measurement error of hydraulic support sensor 0.02m

TABLE 2. The position RMSE of each cutting cycle.

Cutting cycles	RMSE of east(m)		RMSE of north(m)	
	INS/ODO	Assisted by model	INS/ODO	Assisted by model
First	0.886	0.420	0.853	0.180
Second	0.964	0.446	1.002	0.239
Third	0.939	0.592	0.851	0.208
Fourth	0.981	0.663	0.923	0.226
Fifth	1.041	0.816	0.970	0.214

face of the shearer is designed, and the scraper conveyor is composed of 200 chutes. Whenever a cutting cycle is completed, the hydraulic support advances 1m toward the coal body. The whole process simulates five cutting cycles, and the total time is 6.4 hours. The influence of rail kinematics model on the positioning accuracy of the shearer is compared. The simulation settings of the main sensor performance parameters are as follows:

According to the measurement characteristic of the rail kinematics model and the actual motion state of the shearer, the horizontal position of shearer is analyzed. Fig. 6 shows the trajectory comparison between the positioning result with or without the assistance of the rail kinematics model and the real trajectory. Fig. 7 and 8 show the east and north position errors with or without the rail kinematics model, respectively. The trajectory without the assistance of the rail kinematics model has a divergence trend over time in multiple cutting cycles due to the scale factor error and heading angle error of the shearer. The maximum positioning error occurs at the end of each cutting cycle. As listed in Table 2, the Root Mean Square Error (RMSE) of the east direction is 0.886m, 0.964m, 0.939m, 0.98m, 1.041m, and the RMSE of the north direction is 0.853m, 1.002m, 0.851m, 0.923m, 0.970m, respectively. Because the longitudinal displacement of shearer cutting surface is constrained by the measurement of kinematic model, the distance in the first cutting process also restrains the continuous divergence of odometer position recursion as a measurement. Therefore, the divergence of the shearer can be significantly restrained. The RMSE of the east direction is 0.420m, 0.446m, 0.592m, 0.663m, 0.816m, and the RMSE of north direction is 0.18m, 0.239m, 0.208m, 0.226m, 0.214m, respectively. It can be seen from the comparison that the error of the traditional INS/odometer positioning method will continue to increase with the mining of the shearer. However, the proposed algorithm does not diverge significantly in five cutting cycles. The positioning error in each cutting cycle is smaller than that of the traditional algorithm, which significantly improves the positioning accuracy of the shearer.

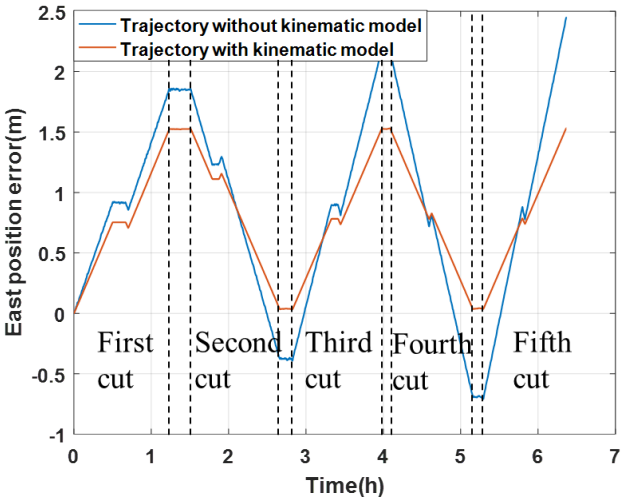

FIGURE 7. Comparison of east position errors.

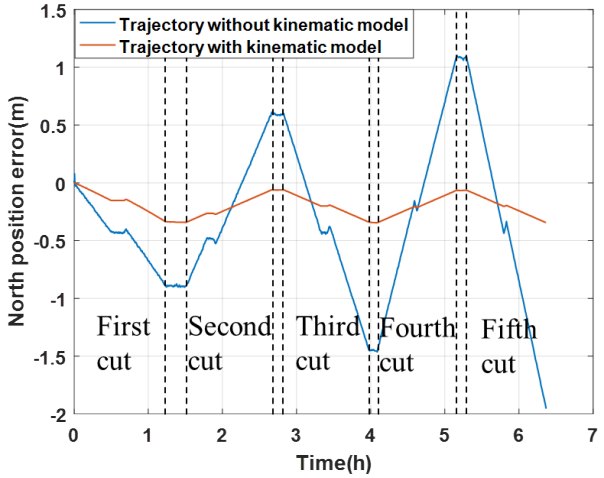

FIGURE 8. Comparison of north position errors.

To improve the reliability of the rail kinematics model and meet the engineering requirements of shearer cutting, the possible faults are simulated to verify the detection and isolation effects of the proposed algorithm on the rail kinematics model. According to the motion characteristics of the rail kinematics model, the simulation injected the measurement deviation with horizontal angle of 1° for every two chutes from 2825s to 3131s. The length of each chute is 1.8m, and the fault formed is shown in Fig. 9. Two different chi-square detection algorithms are used to compare with the algorithm in this paper, namely residual chi-square detection [23] and dual-state chi-square detection [20], which are currently commonly used fault detection methods.

It can be seen from Fig. 10 and Fig. 11 that the fault function detection value and the detection result of the algorithm in this paper can accurately reflect the fault. After the threshold is exceeded, the faulty rail kinematics model is isolated in time. The residual chi-square detection and two-state

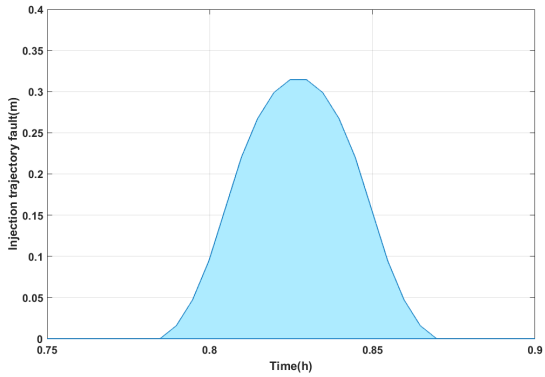

FIGURE 9. Rail kinematics model fault.

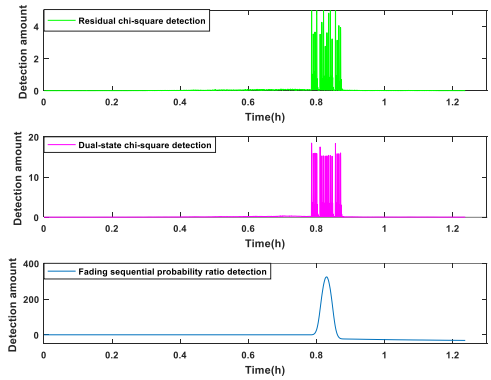

FIGURE 10. Detection amount comparison of residual chi-square detection, dual-state chi-square detection and fading sequential probability ratio detection.

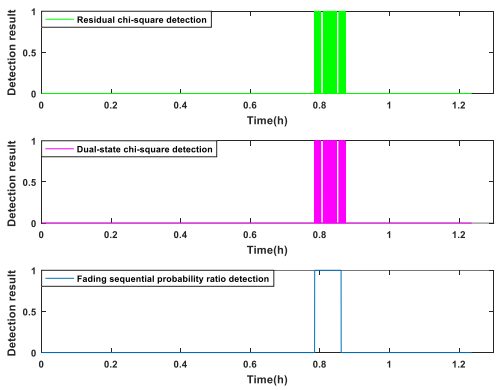

FIGURE 11. Threshold comparison of residual chi-square detection, dual-state chi-square detection and fading sequential probability ratio detection.

chi-square detection are not sensitive to the soft fault, and the fault rail kinematics model will affect the positioning accuracy of the navigation system. It can be seen from Fig. 12 that after the fault measurement is isolated, the north position error does not change significantly. In a relatively short period of time, the odometer can ensure a higher position accuracy of the shearer. Compared with the traditional residual chi-square detection algorithm and state chi-square detection algorithm,

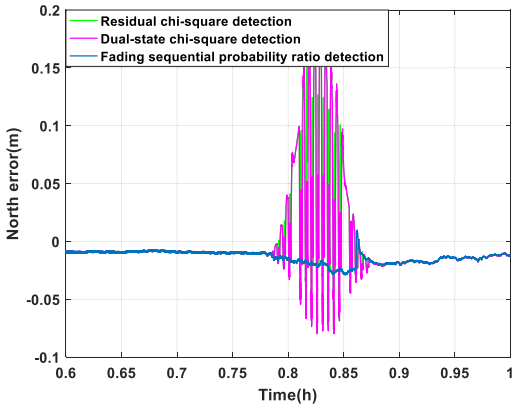

FIGURE 12. North error comparison of residual chi-square detection, dual-state chi-square detection and fading sequential probability ratio detection.

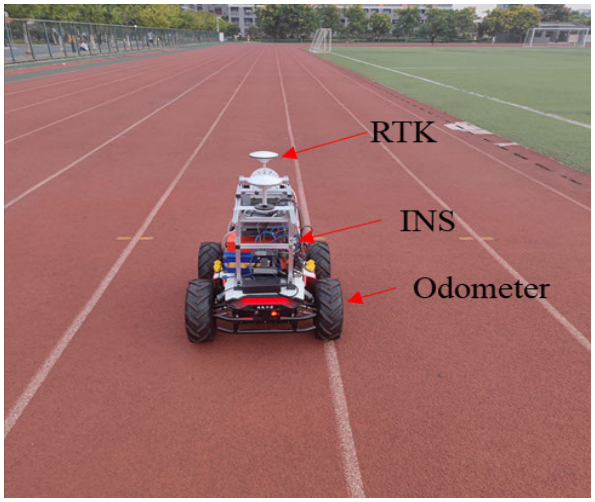

FIGURE 13. Experimental equipment and experiment scene.

the proposed algorithm significantly improves the positioning accuracy of the shearer and ensures the reliability of the system.

B. EXPERIMENTAL VALIDATION

The validity of the algorithm for shearer positioning is further verified by the actual data obtained from the unmanned vehicle. The scenario is shown in Fig. 13. The unmanned vehicle is the Apollo unmanned mobile platform, which is equipped with optical fiber INS, odometer and dual antenna RTK (Real-Time Kinematic). The high precision optical fiber INS is installed in the middle of the unmanned vehicle and the odometer is connected to the wheel of the mobile carrier. The dual antenna RTK is mounted on the top of the vehicle as a reference track. The parameters of each sensor are shown in Table 3. The unmanned vehicle first performed an initial alignment for 5 minutes and then carried out five cutting cycles along the straight line of the playground runway at a speed of about 0.2m/s, which took about 20 minutes.

TABLE 3. Experiment setting of main sensors.

Sensors	Performance parameters
INS	Zero-bias stability of gyro 0.001deg/h Angle random walk of gyro 0.0001deg/sqrt(h) Zero-bias stability of Accelerometers 30 μg
Odometer	Scale factor error 1%
Dual antenna RTK	The positioning accuracy is less than 3cm

Fig. 14 is a comparison of the trajectory with or without the assistance of the rail kinematic model and the reference. Fig. 15 and Fig. 16 are respectively the comparison of the east and north position errors with or without the assistance of rail kinematics model. The errors in both the east and north directions diverge without the assistance of the rail kinematic model. The positioning error diverges faster in the east direction than in the north direction. The main reason is that there is no effective measurement in the cutting direction of the shearer. The change of error conforms to the rule that the error of the INS/odometer integrated navigation system first increases and then decreases during the back-and-forth motion.

TABLE 4. The position RMSE of each cutting cycle.

Cutting cycles	RMSE of east(m)		RMSE of north(m)	
	INS/ODO	Assisted by model	INS/ODO	Assisted by model
First	0.30	0.29	0.90	0.88
Second	0.37	0.28	0.90	0.89
Third	0.53	0.26	0.87	0.82
Fourth	0.69	0.27	0.84	0.82
Fifth	0.88	0.26	0.88	0.80

As shown in Table 4, the east position RMSE of the traditional INS/odometer integrated navigation is 0.30m, 0.37m, 0.53m, 0.69m, 0.88m. and the RMSE of the north direction is 0.90m, 0.90m, 0.87m, 0.84m, 0.88m during the five cutting processes, respectively. Combined with Fig. 17, the positioning method based on the rail kinematics model can effectively suppress the divergence of the heading angle, thereby improving the positioning accuracy in the longitudinal direction between the cutting surfaces. The position RMSE of the proposed algorithm based on the rail kinematics model is 0.29m, 0.28m, 0.26m, 0.27m, 0.26m in the east direction and 0.88m, 0.89m, 0.82m, 0.82m, 0.80m in the west direction respectively in the five cutting processes. The positioning accuracy of the proposed algorithm is significantly higher than that of the traditional INS/odometer integrated navigation.

It is worth noting that the movement of the shearer at the working face is well constrained by the odometer. Because of the round-trip motion, the odometer errors will be partially

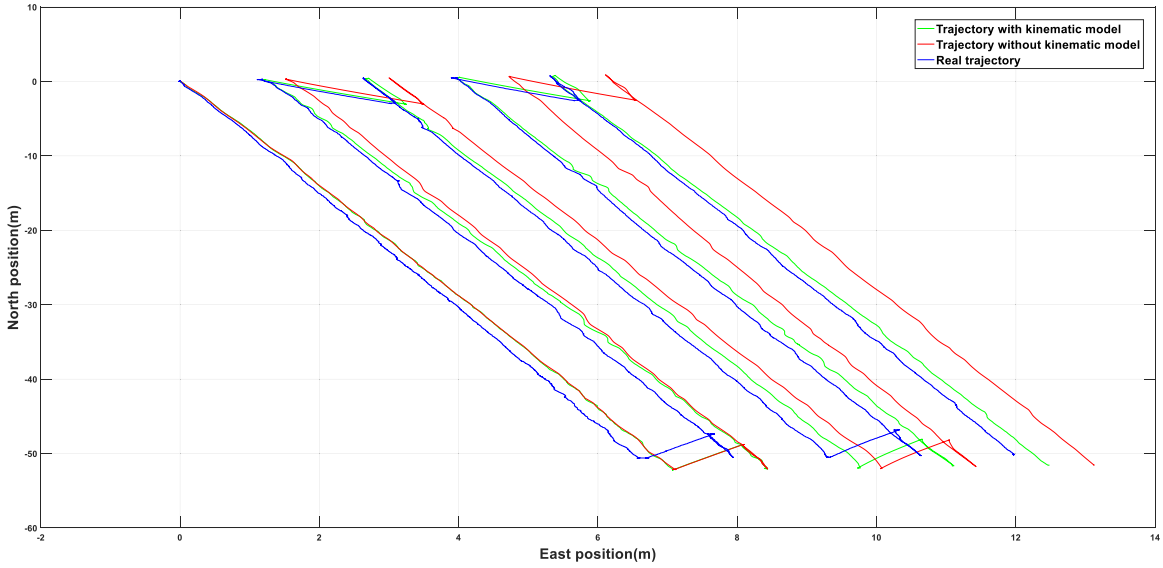

FIGURE 14. Comparison of shearer horizontal cutting trajectory.

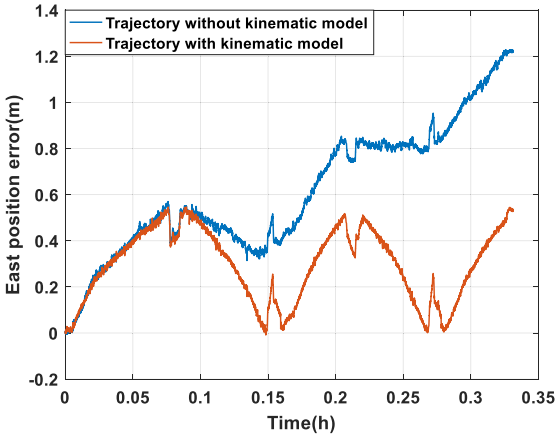

FIGURE 15. Comparison of east position errors.

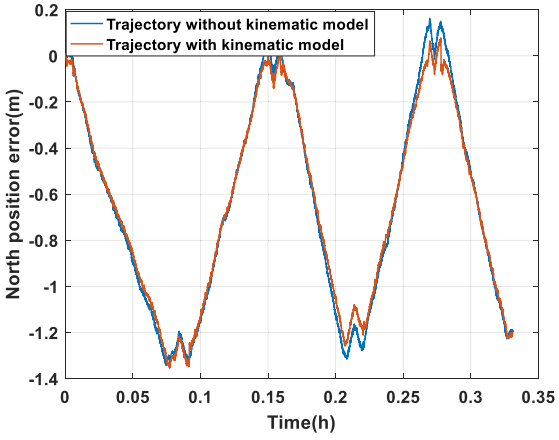

FIGURE 16. Comparison of north position errors.

offset and therefore diverge slowly. Since the heading angle of the vehicle in the experiment is about 172°, the constraint in the north direction is not obvious in the ENU coordinate. In contrast, the constraint in the east direction is better.

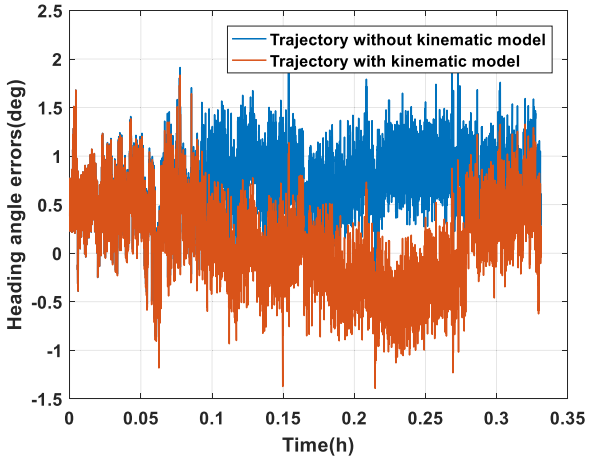

FIGURE 17. Comparison of heading angle error.

According to the effect of the proposed algorithm on fault detection and isolation of the rail kinematics model in the actual environment, the reliability of the model is verified by the experiment. A segment of fault is added to the rail kinematics model mentioned above. The specific detection effect is shown in Fig. 18 and Fig. 19.

As can be seen from Fig. 20, after the fault is identified and isolated, the positioning accuracy is significantly improved. In comparison, the traditional method is not completely isolated from faults, leading to the obvious fluctuation of position errors. The proposed algorithm has better fault identification efficiency compared with traditional residual chi-square detection and two-state Chi-square detection. It can effectively avoid the wrong correction of shearer position caused by model fault and improve underground mining safety.

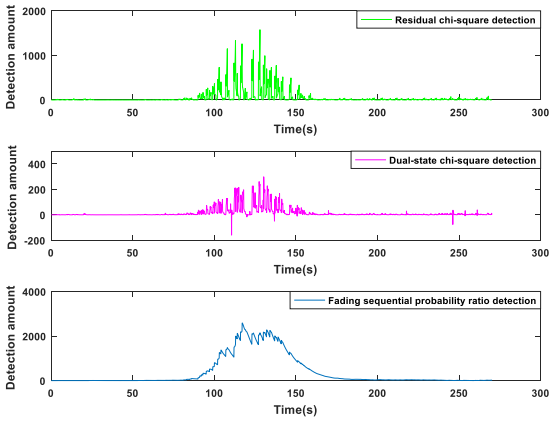

FIGURE 18. Detection amount comparison of residual chi-square detection, dual-state chi-square detection and fading sequential probability ratio detection.

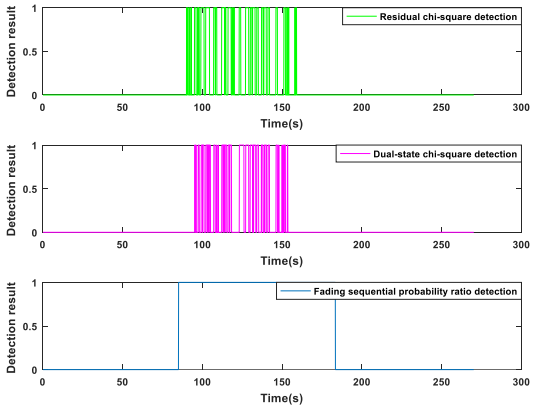

FIGURE 19. Threshold comparison of residual chi-square detection, dual-state chi-square detection and fading sequential probability ratio detection.

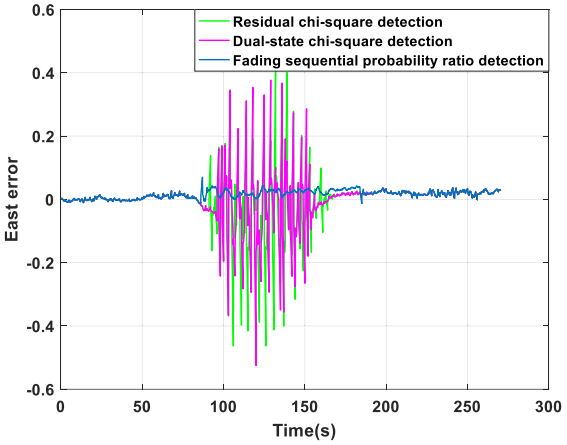

FIGURE 20. East error comparison of residual chi-square detection, dual-state chi-square detection and fading sequential probability ratio detection.

VI. CONCLUSION

A refined rail kinematics model is constructed through analyzing the movement characteristics between the shearer, the scraper conveyor, and the hydraulic support in longwall mining. Combined with the INS and odometer information carried by the shearer, this paper proposes a high-precision positioning algorithm for the shearer based on the rail kinematics model. To deal with the low positioning accuracy caused by the fault of the rail kinematics model, a fault detection and isolation algorithm based on fading sequential probability ratio is proposed. Simulation and experimental results show that the multi-source information fusion by a federated filter with fault detection function can significantly suppress the position divergence of multiple cutting cycles of the shearer without relying on external sensors. When a measurement fault occurs in the rail kinematics model, the fault can be identified and isolated in time, thereby ensuring the positioning accuracy and robustness of the shearer.

REFERENCES

[1] J. C. Ralston, C. O. Hargrave, and M. T. Dunn, "Longwall automation: Trends, challenges and opportunities," *Int. J. Mining Sci. Technol.*, vol. 27, no. 5, pp. 733–739, Aug. 2017.
[2] J. C. Ralston, D. C. Reid, M. T. Dunn, and D. W. Hainsworth, "Longwall automation: Delivering enabling technology to achieve safer and more productive underground mining," *Int. J. Mining Sci. Technol.*, vol. 25, no. 6, pp. 865–876, Nov. 2015.
[3] J. J. Sammarco, "Mining machine orientation using inertial, magnetic, and gravitational sensors," in *Proc. Conf. Rec. IEEE Ind. Appl. Soc. Annu. Meeting*, Oct. 1988, pp. 1260–1262.
[4] D. C. Reid, D. W. Hainsworth, J. C. Ralston, and R. J. McPhee, "Shearer guidance: A major advance in longwall mining," in *Field Service Robotics*. Berlin, Germany: Springer, 2003, pp. 469–476.
[5] S. Wang and S. Wang, "Improving the shearer positioning accuracy using the shearer motion constraints in longwall panels," *IEEE Access*, vol. 8, pp. 52466–52474, 2020.
[6] J. C. Ralston, C. O. Hargrave, and D. W. Hainsworth, "Localisation of mobile underground mining equipment using wireless Ethernet," in *Proc. 14th IAS Annu. Meeting. Conf. Rec. Ind. Appl. Conf.*, Oct. 2005, pp. 225–230.
[7] Q. Fan, W. Li, J. Hui, L. Wu, Z. Yu, W. Yan, and L. Zhou, "Integrated positioning for coal mining machinery in enclosed underground mine based on SINS/WSN," *Scientific World J.*, vol. 2014, pp. 1–12, Jan. 2014.
[8] B. Cao, S. Wang, S. Ge, X. Ma, and W. Liu, "A novel mobile target localization approach for complicate underground environment in mixed LOS/NLOS scenarios," *IEEE Access*, vol. 8, pp. 96347–96362, 2020.
[9] K. You, W. Yang, and R. Han, "The video collaborative localization of a Miner's lamp based on wireless multimedia sensor networks for underground coal mines," *Sensors*, vol. 15, no. 10, pp. 25103–25122, Sep. 2015.
[10] C.-Y. Xu, Y. Song, J.-C. Song, and M.-Q. Tian, "Development of the device to detect the position of coal mining machine by infrared ray based on MCU," *J. China Coal Soc.*, vol. 36, no. S1, pp. 167–170, 2011.
[11] M. T. Dunn, J. P. Thompson, P. B. Reid, and D. C. Reid, "High accuracy inertial navigation for underground mining machinery," in *Proc. IEEE Int. Conf. Autom. Sci. Eng. (CASE)*, Aug. 2012, pp. 1179–1183.
[12] J.-G. Li and K. Zhan, "Intelligent mining technology for an underground metal mine based on unmanned equipment," *Engineering*, vol. 4, no. 3, pp. 381–391, Jun. 2018.
[13] P. B. Reid, M. T. Dunn, D. C. Reid, and J. C. Ralston, "Real-world automation: New capabilities for underground longwall mining," in *Proc. Australas. Conf. Robot. Automat.*, Brisbane, QLD, Australia, Dec. 2010, pp. 1–8.
[14] W. Shibo, Z. Boyuan, W. Shijia, and G. Shirong, "Dynamic precise positioning method of shearer based on closing path optimal estimation model," *IEEE Trans. Autom. Sci. Eng.*, vol. 16, no. 3, pp. 1468–1475, Jul. 2019.
[15] H. Yang, W. Li, C. Luo, J. Zhang, and Z. Si, "Research on error compensation property of strapdown inertial navigation system using dynamic model of shearer," *IEEE Access*, vol. 4, pp. 2045–2055, 2016.
[16] Y. Chen, W. Li, G. Xin, H. Yang, and T. Xia, "An improved strong tracking Kalman filter algorithm for the initial alignment of the shearer," *Complexity*, vol. 2019, pp. 1–12, Mar. 2019.

[17] H. Chung, L. Ojeda, and J. Borenstein, "Accurate mobile robot dead-reckoning with a precision-calibrated fiber-optic gyroscope," *IEEE Trans. Robot. Autom.*, vol. 17, no. 1, pp. 80–84, Feb. 2001.
[18] X. Song, X. Li, W. Tang, W. Zhang, and B. Li, "A hybrid positioning strategy for vehicles in a tunnel based on RFID and in-vehicle sensors," *Sensors*, vol. 14, no. 12, pp. 23095–23118, 2014.
[19] Q. Wang, X. Cui, Y. Li, and F. Ye, "Performance enhancement of a USV INS/CNS/DVL integration navigation system based on an adaptive information sharing factor federated filter," *Sensors*, vol. 17, no. 2, p. 239, 2017.
[20] J. Xu, Z. Xiong, J. Liu, and R. Wang, "A dynamic vector-formed information sharing algorithm based on two-state chi square detection in an adaptive federated filter," *J. Navigat.*, vol. 72, no. 1, pp. 101–120, Jan. 2019.
[21] M. Liu, J. Lai, Z. Li, and J. Liu, "An adaptive cubature Kalman filter algorithm for inertial and land-based navigation system," *Aerosp. Sci. Technol.*, vol. 51, pp. 52–60, Apr. 2016.
[22] G. Gao, S. Gao, X. Peng, and G. Hu, "Fading SPRT method for soft fault diagnosis in SINS/CNS/SRS integrated navigation system," *J. Chin. Inertial Technol.*, vol. 28, no. 6, pp. 834–840, 2020.
[23] R. Wang, Z. Xiong, J. Liu, J. Xu, and L. Shi, "Chi-square and SPRT combined fault detection for multisensor navigation," *IEEE Trans. Aerosp. Electron. Syst.*, vol. 52, no. 3, pp. 1352–1365, Jun. 2016.

XIAOWEI XU was born in Jiangsu, China, in 1992. He received the M.S. degree in electronic and electrical engineering from the University of Leeds, Leeds, U.K., in 2015. He is currently pursuing the Ph.D. degree in automation engineering with the Nanjing University of Aeronautics and Astronautics, Jiangsu. His research interest includes high precision autonomous positioning for underground environments.

JIZHOU LAI was born in Henan, China, in 1977. He received the Ph.D. degree in engineering from the Nanjing University of Aeronautics and Astronautics, in 2005.

Since 2013, he has been a Professor with the School of Automation, Nanjing University of Aeronautics and Astronautics. From 2013 to 2014, he was a Visiting Scholar with the Institute of Aeronautics and Astronautics, University of Toronto, Canada. He is mainly engaged in multi-source integrated intelligent navigation, autonomous navigation without GPS, multi-agent coordination and fault-tolerant navigation, unmanned system intelligent sensing and detection technology, and airborne navigation technology and systems.

Dr. Lai was approved as the China Civil Aviation Science and Technology Innovation Top Talent in 2019 and the 2020 China International "Internet plus" Competition Gold Award Outstanding Instructor.

PIN LV was born in Shandong, China, in 1987. He received the Ph.D. degree in engineering from the Nanjing University of Aeronautics and Astronautics, in 2015. Since 2020, he has been an Assistant Professor with the School of Automation, Nanjing University of Aeronautics and Astronautics. He is mainly engaged in LiDAR SLAM, multi-source integrated intelligent navigation, and autonomous navigation with-out GPS.

JUNQING LU was born in Hubei, China, in 1979. He received the M.S. degree in engineering from the Beijing University of Aeronautics and Astronautics, in 2005. Since 2005, he has been mainly engaged in inertial navigation technology research.

SHIYU BAI was born in Xuzhou, Jiangsu. He is currently pursuing the Ph.D. degree in navigation, guidance, and control with the Nanjing University of Aeronautics and Astronautics, Nanjing, China. His research interests include inertial navigation and multi-sensor fusion localization algorithms for land vehicle and unmanned systems.

HUAFENG HU was born in Hubei, China, in 1986. He received the M.S. degree in engineering from the Beijing University of Aeronautics and Astronautics, in 2013. Since 2013, he has been working with the Hubei Academy of Spaceflight Technology. He is mainly engaged in inertial navigation technology, integrated navigation, and autonomous navigation.